Acta Polytechnica CTU Proceedings **26**:1–6, 2020
doi:10.14311/APP.2020.26.0001

available online at http://ojs.cvut.cz/ojs/index.php/app

HOMOGENIZATION OF UNREINFORCED OLD MASONRY WALL COMPARISON OF SCALAR ISOTROPIC AND ORTHOTROPIC DAMAGE MODELS

Vasco Bernardo, Tomáš Krejčí, Tomáš Koudelka, Michal Šejnoha*

Czech Technical University in Prague, Faculty of Civil Engineering, Department of Mechanics, Thákurova 7, 166 29 Prague 6, Czech Republic

* corresponding author: sejnom@fsv.cvut.cz

Abstract. Masonry is a heterogeneous composite material made of bricks bonded by a mortar matrix. Modeling such a material on macroscale typically calls for homogenization adopting a suitable constitutive model capable of capturing its quasi-brittle behavior. The present contribution concentrates on comparison and potential application of classical isotropic and orthotropic damage models in the framework of strain based first order numerical homogenization. As an illustrative example, a representative volume element in terms of a periodic unit cell is constructed to address the response of an unreinforced masonry (URM) structure typical of "Placa" buildings (mixed masonry-reinforced concrete buildings) built in Portugal. The performance of the two models is examined on the basis of macroscopic stress-strain curves constructed for both tensile and compressive loading. The selected geometrical constraints clearly identify the differences in the predictive capabilities of the two models.

Keywords: Homogenization of unreinforced masonry wall, periodic unit cell, scalar isotropic damage model, orthotropic damage model, "Placa" buildings.

1. Introduction

The Portuguese housing stock results from more than eight centuries of history expansion. The building area consists mostly of residential buildings and it is estimated that half of the existing building stock in Lisbon is represented by old masonry buildings [1]. Four typologies of masonry buildings are typically recognized in the Lisbon Metropolitan Area: buildings built before 1755, "Pombalino" buildings built after the 1755 Earthquake, "Gaioleiro" buildings built between 1870 and 1930 and "Placa" buildings 1930 to 1960 [2].

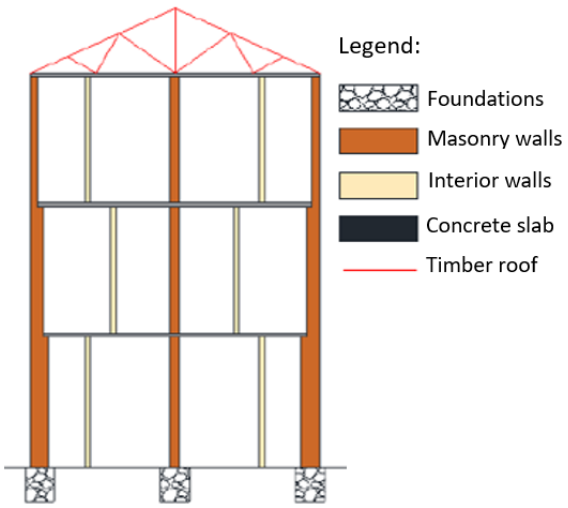

Figure 1. Scheme of "Placa" building typology.

The "Placa" buildings, see Fig. 1, now enjoy a particular interest as they represent 32 % of the Portuguese housing stock [1]. As seen in Fig. 1, the structure consists of a concrete slab simple supported by masonry walls. The exterior walls of these buildings are mainly composed of resistant stone masonry walls or by solid clay bricks with thickness greater than 0.50 m. The interior walls are usually made of solid or hollow clay bricks with thickness up to 0.30 m. The slabs are made of reinforced concrete typically with a total thickness of about 0.10 m and frequently with a single reinforcement layer and poor concrete. Such building experience high vulnerability to damage when subject to seismic loads. This is attributed to insufficient strength or deformation capacity of masonry walls. It is also worth pointing out that no impact of earthquake has been considered in their design as the first Portuguese seismic design regulation appeared not until 1958. Predicting the bearing capacity of such buildings is thus of paramount importance, particularly in areas with a moderate to high seismic risk.

A reliable prediction of the evolution of potential failure due to earthquake then strongly depends on the selected constitutive law for both concrete and masonry. Herein, this issue is addressed in the light of a typically used isotropic scalar damage model [3] and more advanced orthotropic damage model allowing for an independent evolution of damage in three principal strain directions [4]. While concrete is usually assumed isotropic the masonry is only locally isotropic at the level of individual constituents whereas on macroscale it possesses an orthotropic material symmetry. To allow for treating masonry as a homogeneous anisotropic medium thus requires ho-

mogenization. This issue is partially addressed here with reference to one specific topology of a masonry wall linked to the "Placa" building. This choice is supported by available experimental data provided by the National Laboratory for Civil Engineering in Portugal (LNEC) [5, 6].

The paper is organized as follows. Following this introductory part, the two constitutive models are briefly reviewed in Section 2. The basic grounds of the theory of homogenization are introduced next in Section 3. The core of the present work appears in Section 4 devoted to the numerical analysis of unreinforced masonry wall via homogenization. The principal findings are finally summarized in Section 5.

2. Damage models

Generally, damage models distinguish three states of the material - virgin material, damaged material and pseudo-undamaged states. In a virgin state, the material contains no defects and behaves as linearly elastic. At points where the strength limit is exceeded the material experiences damage. In the most simple case of a scalar isotropic damage model, the damage evolution is governed by a dimensionless damage parameter ω written for one-dimensional case as

$$\omega = \frac{A_d}{A}, \tag{1}$$

where A_d is the part of the cross section with evolved defects, i.e with the material in a damaged state and A is the total cross section area. The corresponding stress-strain relation reads

$$\boldsymbol{\sigma} = (1-\omega)\boldsymbol{D}_e\boldsymbol{\varepsilon}, \tag{2}$$

where $\boldsymbol{\sigma}$ is the stress vector, $\boldsymbol{D}_e$ is the elastic stiffness matrix and $\boldsymbol{\varepsilon}$ is the vector of strain components.

The scalar damage parameter $\omega \in [0;1]$ characterizes the material state, where $\omega = 0$ represents an undamaged virgin state, while $\omega = 1$ corresponds to fully evolved defects. The transition states from 0 to 1 are described by the damage evolution law. The present formulation builds on one-dimensional traction-separation law given by [7]

$$\sigma = f_t \exp\left(-\frac{w_{cr}}{u_f}\right), \tag{3}$$

where f_t is the tensile strength, w_{cr} is the crack opening and u_f is the parameter controlling the slope of the softening branch. To partially avoid mesh dependency of the results typical of materials with softening the crack opening is smeared over the element as [7]

$$\kappa - \kappa_e = \omega\kappa = \frac{w_{cr}}{l_{ch}}, \tag{4}$$

where the Mazars equivalent strain κ is provided by

$$\kappa = \sqrt{\sum_{\alpha=1}^{3} H(\varepsilon_\alpha)^2}, \tag{5}$$

where $H(\cdot)$ is the Heaviside function, κ_e is the elastic part of κ and l_{ch} is the element characteristic length. Combining a 1D format of Eq. (2) with Eqs. (4) and (3) and replacing the strain ε with the maximum equivalent strain in the loading history $\bar{\kappa}$ yields the resulting nonlinear equation to be solved for the damage parameter ω

$$(1-\omega)E\bar{\kappa} = f_t \exp\left(-\frac{\omega l_{ch}\bar{\kappa}}{u_f}\right), \tag{6}$$

for states where $\bar{\kappa}$ exceeds the elastic threshold ε_0.

The scalar isotropic damage model can be used successfully for the description of 1D stress states, e.g., 1D tension or bending. A clear drawback is evident from a general multidimensional format of stress-strain relation (2) suggesting the reduction of the entire stiffness matrix even in cases when damage evolves in one direction only. The remedy can be provided by anisotropic [4] or orthotropic damage models. Introducing two independent damage parameters D_α^t and D_α^c for tension and compression, respectively, gives an equivalent format of Eq. (6) now written for individual principal strain directions as

$$\left(1 - D_\alpha^\beta\right) E|\varepsilon_\alpha^\beta| = f_\beta \exp\left(-\frac{D_\alpha^\beta l_{ch}|\varepsilon_\alpha^\beta|}{u_f^\beta}\right), \tag{7}$$

where $\beta \in [t, c]$ identifies either tensile or compressive failure. Further details regarding both models can be found in [8] and [9].

3. Numerical homogenization

In the present study, we limit our attention to a strain based first order homogenization only. To this end, consider a heterogeneous body loaded on its outer boundary by displacement field compatible with a macroscopically uniform strain $\boldsymbol{E}$ in an equivalent homogeneous medium. This allows us in the framework 1st order homogenization to split the local displacement and strain as [10]

$$\Delta\boldsymbol{u}(\mathbf{x}) = \Delta\boldsymbol{E}\,\mathbf{x} + \Delta\boldsymbol{u}^*(\mathbf{x}), \tag{8}$$

$$\Delta\boldsymbol{\varepsilon}(\mathbf{x}) = \Delta\boldsymbol{E} + \Delta\boldsymbol{\varepsilon}^*(\mathbf{x}), \tag{9}$$

where $\boldsymbol{u}^*(\mathbf{x})$ is the fluctuation part of the local displacement field $\boldsymbol{u}(\mathbf{x})$, $\boldsymbol{\varepsilon}^*(\mathbf{x})$ and $\boldsymbol{\varepsilon}(\mathbf{x})$ are the corresponding strains, and $\mathbf{x}$ is the spatial coordinate.

Next, suppose that the computational model is defined in terms of a periodic cell (PUC) taking the actual brick layout into account. For "Placa" building the assumed PUC appears in Fig. 2. The wall thickness is 250 mm, constituted by bricks with nominal dimensions of 250×120×70 mm and 10 mm for the mortar layer.

Because the present formulation assumes the macroscopic strain increment $\Delta\boldsymbol{E}$ in Eq. (8) be prescribed, the solution is searched in terms of the fluctuation rather than total displacements. The stepping stone in deriving $\Delta\boldsymbol{u}^*$ is the Hill lemma written as

$$\left\langle \delta\boldsymbol{\varepsilon}^{\mathrm{T}}(\mathbf{x})\Delta\boldsymbol{\sigma}(\mathbf{x})\right\rangle = 0, \tag{10}$$

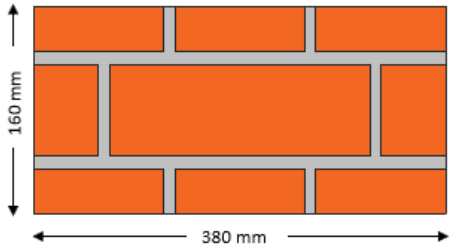

FIGURE 2. Periodic RVE for the masonry wall.

where the left hand side represents the volume average of virtual work done by local stress and strain fields. In the framework of finite element discretization, we approximate $\Delta \boldsymbol{u}^*(\mathbf{x})$ in terms of their nodal values $\Delta \boldsymbol{r}$ to write

$$\Delta \boldsymbol{u}^*(\mathbf{x}) = \mathbf{N}(\mathbf{x})\Delta \boldsymbol{r}, \quad \Delta \boldsymbol{\varepsilon}^*(\mathbf{x}) = \mathbf{B}(\mathbf{x})\Delta \boldsymbol{r}. \tag{11}$$

Substituting from Eq. $(11)_2$ into (10) yields the final system of algebraic equations in the form

$$\mathbf{K}\Delta \boldsymbol{r} = \Delta \boldsymbol{f}, \tag{12}$$

where

$$\mathbf{K} = \frac{1}{\Omega}\int_\Omega \mathbf{B}^{\mathrm{T}}(\mathbf{x})\mathbf{L}(\mathbf{x})\mathbf{B}(\mathbf{x})\ \mathrm{d}\Omega, \tag{13}$$

$$\Delta \boldsymbol{f} = \frac{1}{\Omega}\int_\Omega \mathbf{B}^{\mathrm{T}}(\mathbf{x})\mathbf{L}(\mathbf{x})\Delta \boldsymbol{E}\ \mathrm{d}\Omega, \tag{14}$$

where $\mathbf{L}$ is the material stiffness matrix. It is clear that in order to satisfy

$$\langle \Delta \boldsymbol{\varepsilon}(\mathbf{x}) \rangle = \Delta \boldsymbol{E}, \tag{15}$$

the volume average of the fluctuation part of the displacement field must disappear. This is achieved by adopting the periodic boundary conditions, which in this particular example of a rectangular PUC amount to the same displacements $\boldsymbol{u}^*$ on the opposite boundaries of PUC. The rigid body motion is then constrained by simply fixing the corner displacements.

Note that Eq. (12) can be sought as part of the solution of more complex computational framework based on multiscale analysis illustrated in Fig. 3. In such a case, the actual masonry wall is replaced by an equivalent homogeneous one, so there is no need to consider all the geometrical details on macroscale. Such a distinction between bricks and mortar is made on the mesoscale only being represented by a specific PUC. In case of a fully uncoupled analysis, the theory of homogenization then serves to provide all the necessary data needed in the macroscopic constitutive model. The unit cell simulations then represent a virtual tester to substitute for complex or even unfeasible large scale laboratory experiments. This modeling concept is adopted henceforth providing both the effective elastic properties and various macroscopic stress-strain curves for the selected loading scenarios to compare performance of the two selected models.

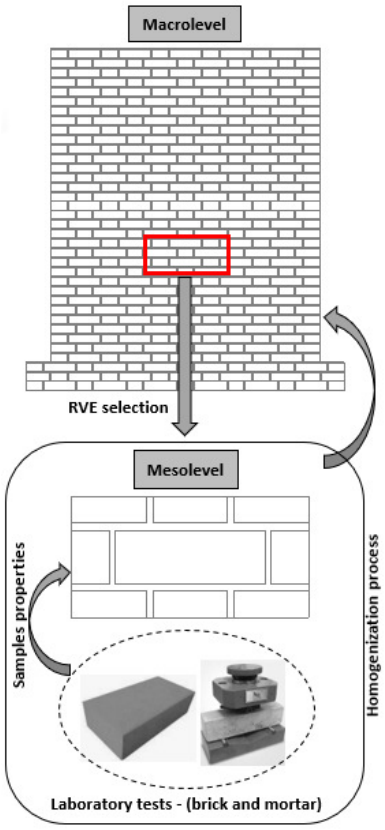

FIGURE 3. Framework for the homogenization of masonry wall.

4. NUMERICAL STUDY

The present section is devoted to the derivation of macroscopic response for various loading scenarios limiting attention to prescribed macroscopic uniform strains, as suggested in Section 3.

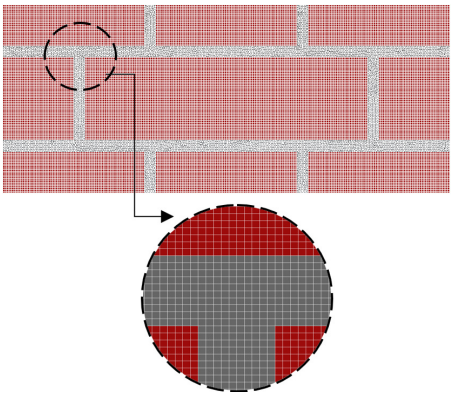

FIGURE 4. Masonry PUC finite element model.

The geometrical model displayed in Fig. 2 is exploited. The corresponding, relatively fine, finite element mesh is plotted in Fig. 4. This mesh consisting of four node quadrilateral elements is used first in the derivation of effective elastic properties and then in the prediction of a nonlinear response when loading the PUC beyond the material elastic limits.

Material	E [GPa]	ν [-]	f_t [MPa]	G_{ft} [N/m]	f_c [MPa]	ρ [kN/m^3]
Brick	13.0	0.2	2.0	58.0	40.0	18.0
Mortar	0.7	0.2	0.1	10.0	1.30	17.5

Table 1. Material parameters of brick and mortar.

4.1. Effective elastic properties from homogenization

The basic prerequisite in the application of homogenization is the knowledge of material data of individual phases as also intimated in Fig. 3. In case of "Placa" masonry, the computational model consists of clay bricks and mortar produced from the cement, lime and sand mixture in the proportions of 1:3. To collect the required properties, the specimens extracted during rehabilitation works from a building located in the center of Lisbon were examined in the National Laboratory for Civil Engineering in Portugal (LNEC), see Fig. 5. The resulting material properties of both phases are listed in Table 1. The same material properties for bed and head joint are assumed. Further details regarding the actual experimental program are available in [5, 6, 11].

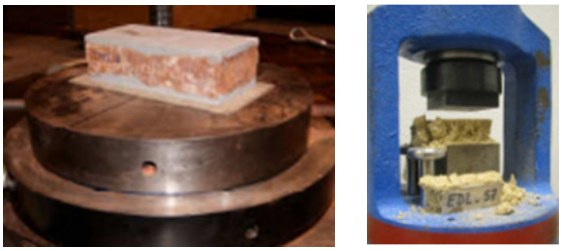

(a) (b)

Figure 5. Axial compression tests: a) Solid clay bricks, b) Mortar [5].

The effective elastic plane-stress stiffness matrix is found first from four independent elasticity solutions when the unit cell is loaded in turn by each of the components of the macroscopic strain $\boldsymbol{E}$ equal to one while the remaining components vanish. The volume averages of the local stress then furnish individual columns of the homogenized effective stiffness matrix, see [12] for further details. The extracted Young's moduli and Poisson's ratios appear in Table 2 clearly identifying the orthotropic material symmetry the "Placa" masonry.

E_{11} [GPa]	E_{22} [GPa]	G_{12} [GPa]	ν_{12} [−]	ν_{21} [−]
6.68	4.03	0.67	0.089	0.147

Table 2. Equivalent elastic properties for RVE.

4.2. Nonlinear response of "Placa" masonry

This section compares the macroscopic nonlinear response of "Placa" masonry due to simple tension and compression applied independently in the X and Y directions as plotted in Fig. 6 also identifying the prescribed components of the macroscopic strain $\boldsymbol{E}$. This is clearly a constrained problem as only one strain component in the principal material direction is assumed nonzero. However, because of heterogeneity all local strain and stress components become active to give rise damage evolution due to tensile failure even in case of compressive loading.

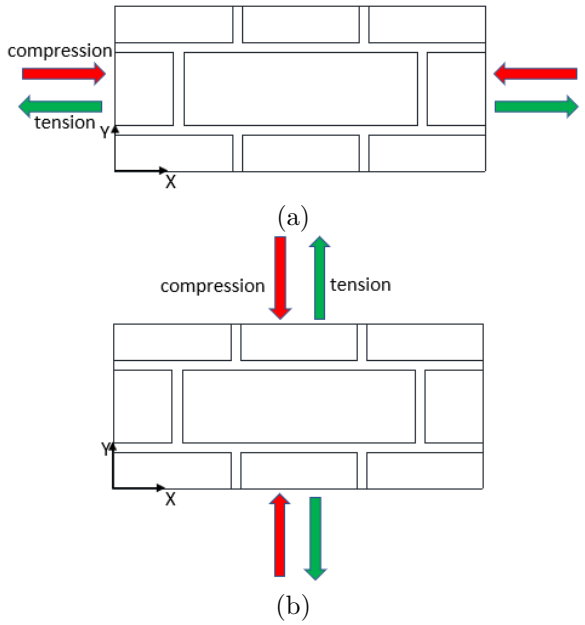

Figure 6. Applied loading: a) $\boldsymbol{E}^{\mathrm{T}} = \{\pm E_{xx}, 0, 0\}$, b) $\boldsymbol{E}^{\mathrm{T}} = \{0, \pm E_{yy}, 0\}$.

The resulting macroscopic stress strain curves ($\boldsymbol{\Sigma}$–$\boldsymbol{E}$) are plotted in Fig. 7. The corresponding damage pattern associated with the last converged step for individual loading conditions appears in Figs. 8 - 11.

It is interesting to point out clear differences between the predictions provided by the two constitutive models observed in Figs. 7(a-c). Particularly the difference in the predicted strength is attributed to the fact that unlike in scalar isotropic damage model the orthotropic damage model reduces the stiffness independently in the principal strain direction according to Eq. (7) providing the condition $|\varepsilon_\alpha^\beta| > \varepsilon_0$ either for tension or compression is met. This is also supported by the evolution of stress component in the direction normal to the applied load. In this con-

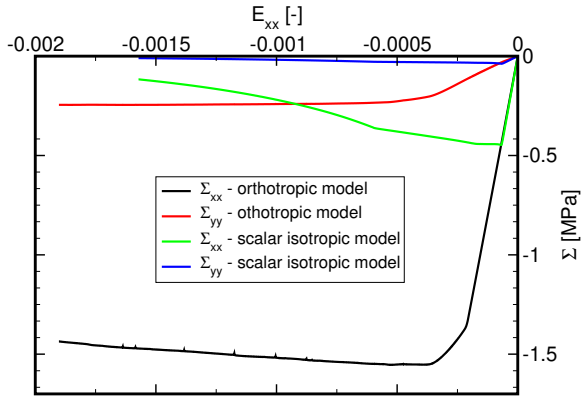

(a)

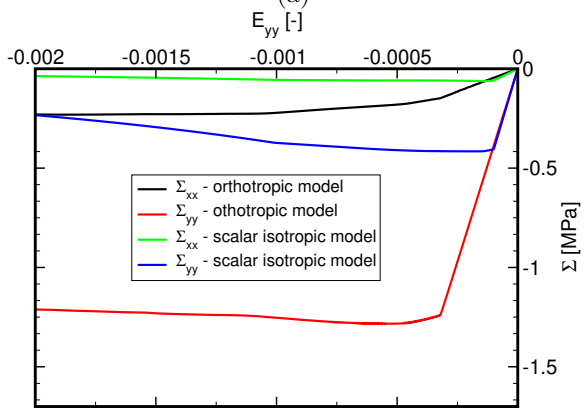

(b)

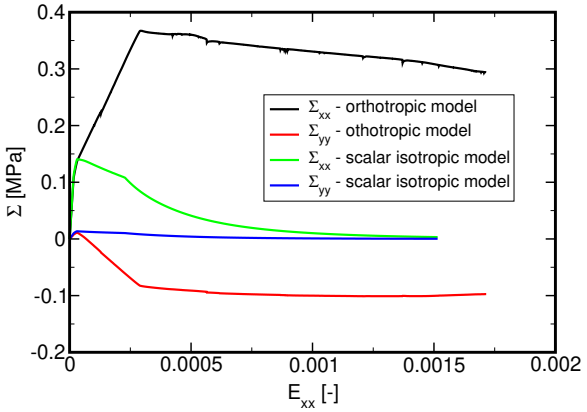

(c)

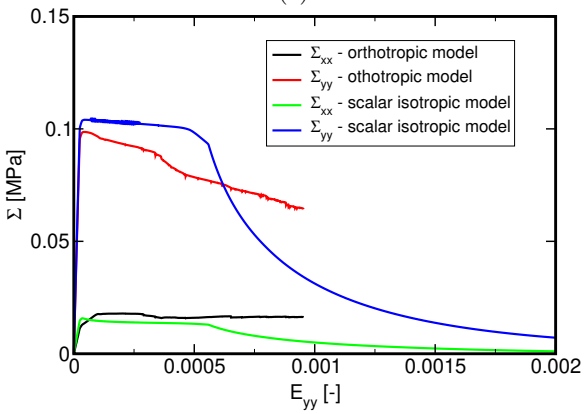

(d)

FIGURE 7. Macroscopic stress-strain curves: a) compression ($E_{xx} < 0$) applied in X direction, b) compression ($E_{yy} < 0$) applied in Y direction, c) tension ($E_{xx} > 0$) applied in X direction, d) tension ($E_{yy} > 0$) applied in Y direction.

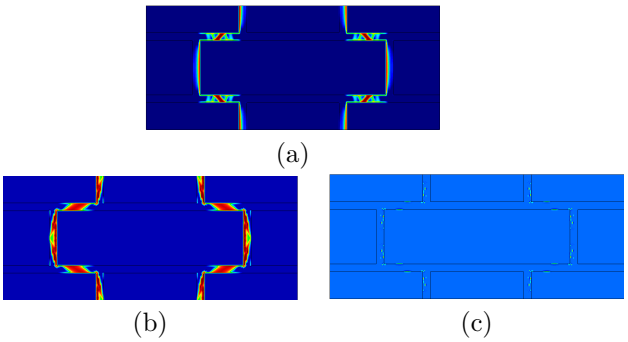

(a) (b) (c)

FIGURE 8. Damage pattern due to $E_{xx} < 0$ (compression): a) isotropic model, b) orthodam-11, c) orthodam-22.

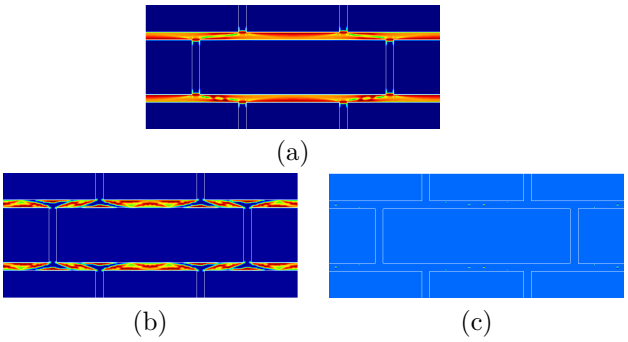

(a) (b) (c)

FIGURE 9. Damage pattern due to $E_{yy} < 0$ (compression): a) isotropic model, b) orthodam-11, c) orthodam-22.

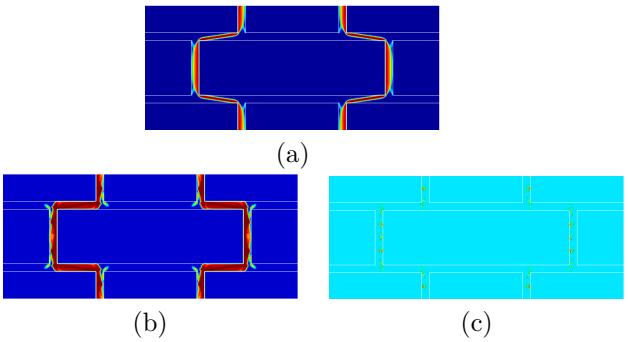

(a) (b) (c)

FIGURE 10. Damage pattern due to $E_{xx} > 0$ (tension): a) isotropic model, b) orthodam-11, c) orthodam-22.

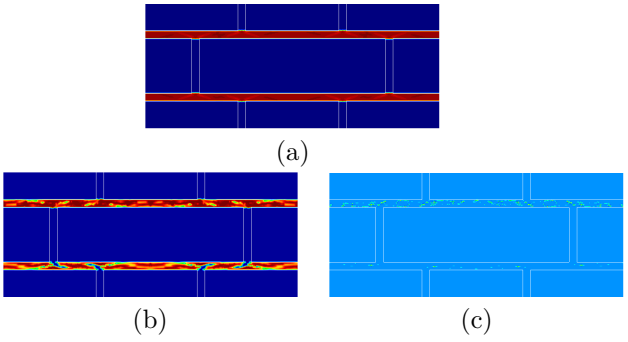

(a) (b) (c)

FIGURE 11. Damage pattern due to $E_{yy} > 0$ (tension): a) isotropic model, b) orthodam-11, c) orthodam-22.

text, the results plotted in Fig. 7(d) should not be surprising once realizing the geometrical arrangement of the PUC. Clearly, if tension is applied along the Y axis, the weak mortar behaves as the weakest link. So, in this case, the stiffness along the X axis, which essentially keeps the original value in case of the orthotropic model, provides no support resulting in a similar behavior predicted by both models.

Although not exactly coincident with the axes of material orthotropy the damage parameter developed in the (11) principal direction (e.g., direction (11) is close to the X direction for the E_{xx} strain component prescribed) is significantly greater in comparison to the one in the second (22) principal direction, which appears negligible.

It should also be mentioned that even though the two macroscopic normal stresses $(\Sigma_{xx}, \Sigma_{yy})$ Figs. 7(a,b) are both compressive due to the applied constraints, e.g. $E_{xx} \neq 0$, while $E_{yy} = 0$, the local failure is in tension because of positive strains developed as a result of material discontinuity and stress concentration at vertices of the brick and mortar interface. This causes the damage pattern in Figs. 8 and 10 and Figs. 9 and 11 be similar. However, because of the geometrical arrangement, the two loading conditions predict different strength limits. But as already mentioned, the maximum compressive stress reached should not be associated with the compressive strength of the masonry material. Given the properties in Table 1, it is not surprising that the damage localizes solely in the mortar phase for all loading scenarios.

5. Conclusions

The present paper was concerned with numerical modeling of masonry structure associated with the "Placa" building in the framework of 1st order homogenization. Apart from the derivation of effective properties of the selected masonry topology the research objectives focused on the prediction of macroscopic response employing two different constitutive models. Limiting attention to tensile failure, the performance of a simple isotropic scalar damage model was compared to more advanced orthotropic damage model. The latter one allows for an independent evolution of damage in three principal directions of the local strain, thus leading in general to more stiff response as illustrated in this for both compression and tension loading condition.

In this regard, the loading was introduced by prescribing the rate of macroscopic strain. Only the loading in principal directions of material orthotropy was considered thus introducing some constraints to the macroscopic response. While such loading conditions appear useful in highlighting the essential differences in the behavior of the two damage models, they cannot be used in the estimation of effective parameters of the macroscopic model such as the tensile strength or the fracture energy in tension. Prediction of such parameters would require combining the stress driven homogenization up to the onset of failure with a specific format of the strain-driven procedure to tract the descending part of the macroscopic stress-strain law consistent with a unidirectional stress state. This study will be the subject of our future research.

Acknowledgements

The financial support supported by the FCT project No.PD/BD/135325/2017 and by the GAČR grant No. 18-24867S is gratefully acknowledged.

References

[1] F. Tiago, J. Milosevic, R. Bento. Seismic vulnerability assessment of a mixed masonry rc building aggregate by linear and nonlinear analyses. *Bulletin of Earthquake Engineering* **14**:1765–2327, 2016.

[2] M. Monteiro, R. Bento. Characterization of "placa" buildings. *ICIST DTC, Portugal* 2012.

[3] G. Mlani, C. Valente, C. Alessandri. The narthex of the church of the Nativity in Bethlehem: A non-linear finite eelement approach to predict the structural damage. *Computers and Structures* **207**:3–18, 2017.

[4] E. Papa, A. Taliercio. Anisotropic Damage Model for the Multiaxial Static and Fatigue Behaviour of Plain Concrete. *Engineering Fracture Mechanics* 1996.

[5] A. I. Marques, P. X. Candeias, M. R. Veiga, J. G. Ferreira. Axial compression and bending tests on old masonry walls. In *3rd International Conference on Protection of historical constructions*. 2017.

[6] A. I. Marques, P. X. Candeias, J. G. Ferreira, M. R. Veiga. Caraterizacao de paredes resistentes de alvenaria antiga. In *REHABEND 2016, Spain*. 2016.

[7] Z. P. Bažant, B. H. Oh. Crack band theory for fracture of concrete. *Matériaux et Construction* **16**(3):155–177, 1983.

[8] T. Krejčí, T. Koudelka, J. Šejnoha, J. Zeman. Computer simulation of concrete structures subject to cyclic temperature loading. In B. H. V. Topping, L. F. Costa Neves, R. C. Barros (eds.), *Proceedings of the Twelfth International Conference on Civil, Structural and Environmental Engineering Computing*. Civil-Comp Press, Stirlingshire, United Kingdom, 2009. Paper 131.

[9] T. Koudelka, T. Krejčí, J. Šejnoha. Analysis of a nuclear power plant containment. In B. H. V. Topping, L. F. Costa Neves, R. C. Barros (eds.), *Proceedings of the Twelfth International Conference on Civil, Structural and Environmental Engineering Computing*. Civil-Comp Press, Stirlingshire, United Kingdom, 2009. Paper 132.

[10] J. C. Michel, H. Moulinec, P. Suquet. Effective properties of composite materials with periodic microstructure: A computational approach. *Computer Methods in Applied Mechanics and Engineering* **172**:109–143, 1999.

[11] A. I. Marques, P. X. Candeias, J. G. Ferreira, M. R. Veiga. Ensaios de compressao diagonal em paredes antigas de alvenaria de tijolo. In *CONSTRUCAO 2018, Porto*. 2018.

[12] M. Šejnoha, J. Zeman. *Micromechanics in Practice*. WIT Press, Southampton, Boston, 2013.